Geophysical Prospecting, 2000, **48**, 521–537

Non-equilibrium compaction and abnormal pore-fluid pressures: effects on rock properties[1]

José M. Carcione[2] and Anthony F. Gangi[3]

Abstract

Knowledge of pore pressure using seismic data will help in planning the drilling process to control potentially dangerous abnormal pressures. Various physical processes cause anomalous pressures on an underground fluid. Non-equilibrium compaction is a significant process of overpressure generation. This occurs when the sedimentation rate is so rapid that the pore fluids do not have a chance to 'escape' from the pore space.

The model assumes a closed system and that the pore space is filled with water and hydrocarbon in a liquid state. Balancing mass and volume fractions yields the fluid pressure versus time of deposition and depth of burial. Thermal effects are taken into account. The pore pressure, together with the confining pressure, determines the effective pressure which, in turn, determines the bulk moduli of the rock matrix.

We assume a sandstone saturated with hydrocarbons and water, for which calibration of the model with experimental data is possible. The seismic velocities and attenuation factors are computed by using Biot's theory of dynamic poroelasticity and the generalized linear solid. The example shows that the formation can be overpressured or underpressured depending on the properties of the saturating fluid. Wave velocities and quality factors decrease with decreasing differential pressure. The effect is important below approximately 20 MPa. The model is in good agreement with experimental data for Berea sandstone and provides a tool for predicting pore pressure from seismic attributes.

Introduction

Non-equilibrium compaction or mechanical compaction disequilibrium is a consequence of a rapid deposition compared to the rate of expelling pore fluids by

[1]Paper presented at the 61st EAGE Conference – Geophysical Division, Helsinki, Finland, June 1999. Received November 1998, revision accepted October 1999.
[2]Osservatorio Geofisico Sperimentale, PO Box 2011, Opicina, 34016 Trieste, Italy. E-mail: jcarcione@ogs.trieste.it
[3]Department of Geology and Geophysics, Texas A&M University, College Station, TX 77843-3114, USA. E-mail: gangi@tamu.edu

gravitational compaction. In this situation, the fluids carry part of the load that would be held by grain contacts and abnormal pore pressures develop in the pore space. A description of this overpressure mechanism was given by Rubey and Hubbert (1959) and mathematical treatments of the problem have been provided, for instance, by Bredehoeft and Hanshaw (1968), Smith (1971) and Dutta (1983). These models use Darcy's law and their predictions are greatly affected by the choice of the constitutive relationships between porosity, permeability and effective stress. Dutta (1983) illustrated how the predicted geopressure profiles depend dramatically on the assumed permeability-versus-porosity models (see also Dutta and Levin 1990).

The approach presented here assumes that if the rock is a shale, its permeability is extremely low, and if the rock is a sandstone, there are impermeable sealing faults and surrounding layers so that the fluids cannot escape from the pore space. We assume a simple basin-evolution model with a constant sedimentation rate and a constant geothermal gradient. The disequilibrium compaction is started at a given depth, with the pores filled with liquid hydrocarbon and water. The hydrocarbon ranges from relatively light oils to heavy oils, with no dissolved gas (i.e. dead oils). Balancing mass and volume fractions in the pore space yields the pore pressure, the saturations and the porosity versus time and depth of burial. Thermal effects are also taken into account. The pore pressure, together with the confining pressure, determines the effective pressure which, in turn, determines the bulk moduli of the rock matrix.

Seismic velocities have been extensively used to predict pore pressure, with most of the models based on empirical relationships (Dutta and Levin 1990). Attenuation has been studied mainly at ultrasonic frequencies, and a few works have focused on VSP data and sonic data (e.g. Hague 1981; Dasios, Astin and McCann 1998a). Recently, attenuation obtained from surface seismic data has been successfully used to predict lithology and pore pressure (Helle *et al.* 1993; Dasios, Astin and McCann 1998b). In this work, the seismic properties are calculated using a modification of Biot's theory for fully saturated porous solids. The effective parameters for the fluid mixture are computed by the average formulae given by Berryman, Thigpen and Chin (1988). The wave velocities of the dry rock, determined by laboratory measurements, give estimates of its pore compressibility and bulk moduli in the low-frequency (relaxed) regime. Since dissipation mechanisms are mainly caused by grain/fluid interactions, dry-rock velocities are, in principle, frequency-independent. On the other hand, measurements of ultrasonic wet-rock velocities provide the high-frequency limit (unrelaxed) velocities, which can be used to estimate the amount of velocity dispersion between the seismic and ultrasonic ranges and, therefore, the amount of attenuation. Using this information, the phase velocities and attenuation factors are computed as a function of pore pressure and frequency.

Non-equilibrium compaction

Let us assume a geological formation, as for instance a shale or a sealed sandstone unit, at depth z. The lithostatic pressure p_c for an average sediment density ρ is equal

to $p_c = \rho g z$, where g is the acceleration due to gravity. On the other hand, the hydrostatic pore pressure is approximately $p_H = \rho_w g z$, where ρ_w is the density of water.

For a constant sediment burial rate S and a constant geothermal gradient G, the temperature variation of a particular sediment volume is

$$T = T_0 + Gz, \qquad z = St, \tag{1}$$

where t is the deposition time and T_0 is the surface temperature. Typical values of G range from 10 to 30°C/km, while S may range between 0.05 and 3 km/m.y. (m.y. = million years) (Mann and Mackenzie 1990).

The case of non-equilibrium compaction is that in which the sedimentation rate is so rapid that the pore fluids do not have a chance to 'escape'. Then, assuming only liquid hydrocarbon and water in the pore space,

$$V_p = V_o + V_w, \tag{2}$$

where V_p is the pore volume, and V_o and V_w are the volumes of the hydrocarbon and water in the pore space, respectively, we have

$$\mathrm{d}V_p(p_e, T, M_p) = \mathrm{d}V_o(p, T, M_o) + \mathrm{d}V_w(p, T, M_w), \tag{3}$$

where p_e is the effective pressure, p is the pore pressure, M_o and M_w are the masses of the hydrocarbon and water phases and M_p is the total mass in the pore space.

In general, seismic properties, such as wave velocity and attenuation, depend on the effective pressure, given by

$$p_e = p_c - np, \tag{4}$$

where p_c is the confining pressure and $n \leq 1$ is the effective-pressure coefficient. Note that the effective pressure equals the confining pressure at zero pore pressure. It is found that $n \approx 1$ for static measurements of the compressibilities (Zimmerman, Somerton and King 1986), while n is approximately linearly dependent on the differential pressure $p_d = p_c - p$ in dynamic experiments (Gangi and Carlson 1996; Prasad and Manghnani 1997), i.e.

$$n \simeq n_0 - n_1 p_d, \tag{5}$$

where n_0 and n_1 are constant coefficients.

If no mass (of the hydrocarbon or the water) leaves the pore space (and there is no 'phase' conversion), then $\mathrm{d}M_p = 0 = \mathrm{d}M_o = \mathrm{d}M_w$ and we have

$$\mathrm{d}V_p = \left(\frac{\partial V_p}{\partial p_e}\right)\mathrm{d}p_e + \left(\frac{\partial V_p}{\partial T}\right)\mathrm{d}T = \left(\frac{\partial V_o}{\partial p} + \frac{\partial V_w}{\partial p}\right)\mathrm{d}p + \left(\frac{\partial V_o}{\partial T} + \frac{\partial V_w}{\partial T}\right)\mathrm{d}T, \tag{6}$$

with

$$c_p = -\frac{1}{V_p}\frac{\mathrm{d}V_p}{\mathrm{d}p_e}, \qquad c_o = -\frac{1}{V_o}\frac{\mathrm{d}V_o}{\mathrm{d}p}, \qquad c_w = -\frac{1}{V_w}\frac{\mathrm{d}V_w}{\mathrm{d}p}, \tag{7}$$

$$\alpha_p = \frac{1}{V_p}\frac{dV_p}{dT}, \qquad \alpha_o = \frac{1}{V_o}\frac{dV_o}{dT}, \qquad \alpha_w = \frac{1}{V_w}\frac{dV_w}{dT}, \tag{8}$$

as the compressibilities and thermal expansion coefficients for the pore space, hydrocarbon and water.

Let $dp_c = \rho g\, dz$ be the change in overburden or confining pressure, where dz is the increment in depth or depth change. A rough estimation of the condition for overpressure can be obtained by assuming $n \approx 1$. Then, $dp_e \approx dp_c - dp$, and we get

$$-(c_p V_p)\, dp_e + (c_o V_o + c_w V_w)\, dp = (-\alpha_p V_p + \alpha_o V_o + \alpha_w V_w)\, dT \tag{9}$$

or

$$(c_p V_p + c_o V_o + c_w V_w)\, dp - c_p V_p \rho g\, dz = (-\alpha_p V_p + \alpha_o V_o + \alpha_w V_w) G\, dz, \tag{10}$$

where $G = dT/dz$ is the geothermal gradient. Therefore, we have

$$\frac{dp}{dz} = \frac{c_p V_p \rho g + (-\alpha_p V_p + \alpha_o V_o + \alpha_w V_w) G}{c_p V_p + c_o V_o + c_w V_w} \tag{11}$$

or

$$\frac{dp}{dz} = \frac{c_p \rho g + [-\alpha_p + \alpha_o (1 - S_w) + \alpha_w S_w] G}{c_p + c_o (1 - S_w) + c_w S_w}, \tag{12}$$

where $S_w = V_w/V_p$ is the water saturation in the pore space.

If all the parameters are made independent of depth, this equation gives overpressures as a function of depth if $dp/dz > g\rho_w$, where ρ_w is the density of water. The inequality holds for the following condition on the pore compressibility,

$$c_p > \frac{c_o S_o + c_w S_w - (\alpha_o S_o + \alpha_w S_w - \alpha_p) G/(g\rho_w)}{\rho/\rho_w - 1}. \tag{13}$$

Neglecting thermal effects (i.e. letting $\alpha_o S_o + \alpha_w S_w - \alpha_p = 0$), the condition becomes $c_p > (c_o S_o + c_w S_w)/(\rho/\rho_w - 1)$. For instance, assuming $S_w = 1$, $\rho = 2400\,\mathrm{kg/m^3}$ and $\rho_w = 1040\,\mathrm{kg/m^3}$ gives $c_p > 0.76\, c_w$. This fact indicates that non-equilibrium compaction can be a possible overpressure mechanism.

Excess pore pressure versus depth

We assume that the compressibilities of the hydrocarbon and water are independent of pressure and temperature. That this is the case can be seen from the results given by Batzle and Wang (1992) in their Figs 5 and 13, where they show that the density is almost a linear function of temperature and pressure. This means that the coefficients mentioned are approximately constant (see also their Fig. 7, where the hydrocarbon compressibility is almost constant when going from low temperature and low pressure to high temperature and high pressure). Moreover, we assume that the rock compressibility is independent of temperature but depends on pressure. We consider

the following functional form for c_p as a function of effective pressure:

$$c_p = c_p^{\infty} + \beta \exp(-p_e/p^{\star}), \tag{14}$$

where c_p^{∞}, β and $p^{\star}$ are coefficients obtained by fitting the experimental data. Assume that at an initial time t_i, corresponding to depth z_i, the volume of rock behaves as a closed system. That is, if the unit is a shale, its permeability is extremely low, and if the unit is a sandstone, the permeability of the sealing faults and surrounding layers is sufficiently low so that the rate of pressure increase greatly exceeds the dissipation of pressure by flow. Pore pressure excess is measured relative to hydrostatic pressure.

Integration of (7) and (8) from p_i (p_{ei}) to p (p_e) and T_i to $T_i + \Delta T$, where $\Delta T = T - T_i$, yields

$$V_o(p, T) = V_{oi}[\exp(-c_o \Delta p + \alpha_o \Delta T)], \tag{15}$$

$$V_w(p, T) = V_{wi}[\exp(-c_w \Delta p + \alpha_w \Delta T)] \tag{16}$$

and

$$V_p(p, T) = V_{pi}\{\exp[E(\Delta p) + \alpha_p \Delta T]\}, \tag{17}$$

where (equation (14))

$$E(\Delta p) = -c_p^{\infty} \Delta p_e + \beta p^{\star}[\exp(-p_e/p^{\star}) - \exp(-p_{ei}/p^{\star})],$$

and $\Delta p_e = p_e - p_{ei}$ and $\Delta p = p - p_{Hi}$, $p_{Hi} = \rho_w g z_i$, since $p_i = p_{Hi}$.

Using (5), the effective pressure (4) can be written as

$$p_e = p_c - (n_0 - n_1 p_c)p - n_1 p^2. \tag{18}$$

The pore volume at pore pressure p and temperature T is given by

$$V_p(p, T) = V_{pi}\{\exp[E(\Delta p) + \alpha_p \Delta T]\} = V_{wi}[\exp(-c_w \Delta p + \alpha_w \Delta T)] + V_{oi}[\exp(-c_o \Delta p + \alpha_o \Delta T)]. \tag{19}$$

Since the initial saturations are

$$S_{wi} = V_{wi}/V_{pi}, \qquad S_{oi} = V_{oi}/V_{pi} = 1 - S_{wi}, \tag{20}$$

(19) becomes

$$\exp[E(\Delta p) + \alpha_p \Delta T] = S_{wi}[\exp(-c_w \Delta p + \alpha_w \Delta T)] + (1 - S_{wi})[\exp(-c_o \Delta p + \alpha_o \Delta T)]. \tag{21}$$

The solution of (21) gives the pore pressure p as a function of depth and deposition time t, with $\Delta T = T - T_i = G(z - z_i) = GS(t - t_i)$ for a constant geothermal gradient and a constant sediment burial rate. The excess pore pressure is $p - p_H$. It is important to point out that, unlike other models for compaction disequilibrium (Mann and Mackenzie 1990), the present model is not sensitive to the deposition rate S, since we assume a closed 'system', that is, the fluids cannot be squeezed out of the

rock volume. The magnitude of the abnormal pressures depends mainly on the compressibilities of the rock frame (i.e. the dry rock) and pore fluids.

Saturations and porosities versus excess pressure

As the pore pressure increases from p_i to p, the pore volume changes from V_{pi} to $V_{pi}\{\exp[E(\Delta p) + \alpha_p \Delta T]\}$. The saturations are equal to the corresponding volumes divided by the pore volume. Using (15), (16), (17) and (20) gives, for the hydrocarbon and water saturations,

$$S_o = (1 - S_{wi})[\exp(-c_o \Delta p + \alpha_o \Delta T - E(\Delta p) - \alpha_p \Delta T)] \tag{22}$$

and

$$S_w = S_{wi}[\exp(-c_w \Delta p + \alpha_w \Delta T - E(\Delta p) - \alpha_p \Delta T)], \tag{23}$$

respectively. On the other hand, the hydrocarbon and water fractions are

$$\phi_o = \phi S_o, \qquad \phi_w = \phi S_w, \tag{24}$$

where ϕ is the total porosity, given by

$$\phi = \frac{V_p}{V_p + V_s},$$

with V_s denoting the volume of the solid part. This can be calculated from the initial porosity ϕ_i, since $\phi_i = V_{pi}/(V_{pi} + V_s)$. Thus, $V_s = V_{pi}(1/\phi_i - 1)$ and, using (17), we obtain

$$\phi = \frac{\phi_i \exp[E(\Delta p) + \alpha_p \Delta T]}{1 + \phi_i\{\exp[E(\Delta p) + \alpha_p \Delta T] - 1\}}. \tag{25}$$

Defining ϕ_s as the mineral matrix fraction, we have

$$\phi_s = 1 - \phi. \tag{26}$$

Compressibility and dry-rock bulk moduli

In sandstones, the pore compressibility c_p is closely related to the bulk modulus of the matrix K_m (the compressibility c_p is denoted by C_{pp} by Zimmerman *et al.* (1986) and by $K^{-1}_{\phi p}$ by Mavko and Mukerji (1995), and K_m corresponds to C^{-1}_{bc} and K^{-1}_{dry}, respectively). Using the present notation, c_p can be expressed as

$$c_p = \left(\frac{1}{K_m} - \frac{1}{K_s}\right)\frac{1}{\phi} - \frac{1}{K_s}, \tag{27}$$

where K_s is the bulk modulus of the solid grains and ϕ depends on the excess pore pressure $p - p_H$. Since dry-rock wave velocities are practically frequency-independent, the seismic bulk moduli K_m and μ_m versus effective pressure can be obtained from laboratory measurements in dry samples. If V_{P0} and V_{S0} are the experimental compressional- and shear-wave velocities, the moduli are given approximately by

$$K_m = (1 - \phi)\rho_s\left(V_{P0}^2 - \frac{4}{3}V_{S0}^2\right), \qquad \mu_m = (1 - \phi)\rho_s V_{S0}^2, \tag{28}$$

where ρ_s is the grain density and ϕ is the porosity. We recall that K_m is the rock modulus at constant pore pressure, i.e. the case when the bulk modulus of the pore fluid is negligible compared with the frame bulk modulus, as for example air at room conditions (Mavko and Mukerji 1995).

Seismic properties of a porous medium saturated with hydrocarbon and water

Biot's theory of dynamic poroelasticity is used to compute the wave velocities and attenuation factors, where the pore fluid is a mixture of hydrocarbon and water. The complex velocities of the fast (+sign) and slow (−sign) compressional waves and shear wave are (see e.g. Carcione 1998),

$$V_{P\pm}^2 = \frac{A \pm \sqrt{A^2 - 4M_c E\rho_c\rho^\star}}{2\rho_c\rho^\star} \tag{29}$$

and

$$V_S^2 = \frac{\mu}{\rho_c}, \tag{30}$$

where

$$A = M_c(\rho - 2\alpha\rho_f) + \rho^\star(E + \alpha^2 M_c), \tag{31}$$

$$\rho_c = \rho - \rho_f^2/\rho^\star \tag{32}$$

and

$$\rho^\star = \frac{\mathcal{T}}{\phi}\rho_f - \frac{\mathrm{i}}{2\pi f}\frac{\eta}{\kappa}, \tag{33}$$

with M_c denoting the complex and frequency-dependent modulus between the solid matrix and the fluid mixture, α and E denoting elastic coefficients, f denoting the frequency and $\mathrm{i} = \sqrt{-1}$. The sediment density is

$$\rho = (1 - \phi)\rho_s + \phi\rho_f,$$

where ρ_s and ρ_f are the solid and fluid densities, respectively; $\mathcal{T}$ is the tortuosity, η is the fluid viscosity and κ is the permeability of the medium.

The elastic coefficients are given by

$$E = K_{\rm m} + \frac{4}{3}\mu, \tag{34}$$

$$M = \frac{K_{\rm s}^2}{D - K_{\rm m}}, \tag{35}$$

$$D = K_{\rm s}[1 + \phi(K_{\rm s}K_{\rm f}^{-1} - 1)], \tag{36}$$

$$\alpha = 1 - \frac{K_{\rm m}}{K_{\rm s}}, \tag{37}$$

with $K_{\rm f}$ denoting the bulk modulus of the hydrocarbon/water mixture. The stiffness E is the P-wave modulus of the dry skeleton, M is the elastic coupling modulus between the solid and the fluid, and α is the poroelastic coefficient of effective stress.

Biot's theory successfully describes the wave propagation properties of synthetic porous media such as sintered glass beads. In natural porous media such as sandstone, discrepancies between Biot's theory and measurements are due to complex pore shapes that are not present in simple synthetic media (Gist 1994). Skeleton-fluid mechanisms are modelled by generalizing the coupling modulus M to a time-dependent relaxation function, based on a continuous distribution of relaxation mechanisms. This model provides a constant quality factor over a broad frequency band. In this case, $M_{\rm c}$ is generalized to a frequency-dependent modulus of the form,

$$M_{\rm c} = M\left[1 + \frac{2}{\pi\bar{Q}}\ln\left(\frac{1 + {\rm i}\omega\tau_2}{1 + {\rm i}\omega\tau_1}\right)\right]^{-1}, \tag{38}$$

where τ_1 and τ_2 are time constants, with $\tau_2 < \tau_1$, and $\bar{Q}$ defines the value of the quality factor, which remains nearly constant over the selected frequency band. The low-frequency limit of $M_{\rm c}$ is the Biot modulus M.

The hydrocarbon/water mixture behaves as a composite fluid with properties depending on the constants of the constituents and their relative concentrations. This problem has been analysed by Berryman *et al.* (1988) and the results are given by the formulae

$$K_{\rm f} = (S_{\rm o}c_{\rm o} + S_{\rm w}c_{\rm w})^{-1}, \tag{39}$$

$$\rho_{\rm f} = S_{\rm o}\rho_{\rm o} + S_{\rm w}\rho_{\rm w}, \tag{40}$$

where $\rho_{\rm o}$ is the density of the hydrocarbon,

$$\eta_{\rm f} = S_{\rm o}\eta_{\rm o} + S_{\rm w}\eta_{\rm w}, \tag{41}$$

where $\eta_{\rm o}$ and $\eta_{\rm w}$ are the viscosities of the hydrocarbon and water, respectively. Equation (41) is a good approximation for most values of the saturations.

Biot's theory is strictly valid for frequencies below

$$f_{\rm c} = \frac{\eta_{\rm f}\phi}{2\pi\mathcal{T}\rho_{\rm f}\kappa}. \tag{42}$$

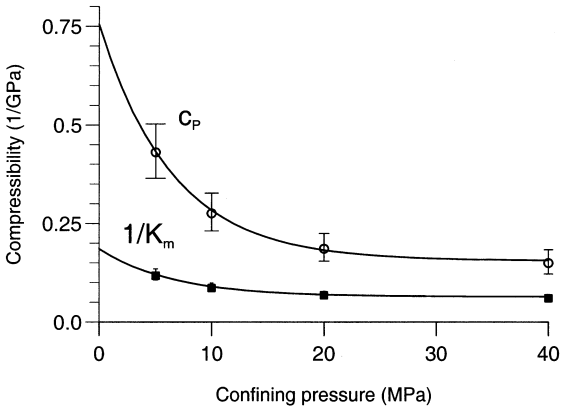

Figure 1. Best-fit plots of c_p and K_m^{-1} obtained from the experimental data for Berea sandstone published by Winkler (1985, Figs 3 and 4, and Tables 4 and 7).

The phase velocity c is equal to the angular frequency $\omega = 2\pi f$ divided by the real wavenumber. Then,

$$c_{P\pm} = \left[\mathrm{Re}\left(\frac{1}{V_{P\pm}}\right)\right]^{-1}, \qquad c_S = \left[\mathrm{Re}\left(\frac{1}{V_S}\right)\right]^{-1}, \tag{43}$$

where Re denotes the real part.

Following the single-phase case, we assume that the fast-wave quality factor takes the form,

$$Q_p = \frac{\mathrm{Re}(V_{P+}^2)}{\mathrm{Im}(V_{P+}^2),} \tag{44}$$

where Im denotes the imaginary part.

Example

We assume a sandstone saturated with oil and water, since the determination of dry-rock bulk moduli for shales is extremely difficult. Even for sandstones, there are few laboratory data to calibrate the model. With a surface temperature of 25°C, a temperature gradient $G = 10°\mathrm{C/km}$, a sedimentation rate $S = 0.08\,\mathrm{km/m.y.}$ and a reservoir volume at $z_i = z_1 = 2\,\mathrm{km}$, we have $t_i = t_1 = 25\,\mathrm{m.y.}$ and $T_1 = 45°\mathrm{C}$. After 75 m.y., the depth of burial is $z_2 = 8\,\mathrm{km}$, $t_2 = 100\,\mathrm{m.y.}$ and $T_2 = 105°\mathrm{C}$. On the other hand, if $\rho = 2400\,\mathrm{kg/m^3}$, the confining pressure has increased from $p_{c1} = 47\,\mathrm{MPa}$ to approximately $p_{c2} = 188\,\mathrm{MPa}$, and the initial pore pressure is $p_i \simeq 20\,\mathrm{MPa}$ (assuming $\rho_w = 1000\,\mathrm{kg/m^3}$). If no disequilibrium compaction takes place, the final pore pressure would be the hydrostatic pressure at 8 km, i.e. approximately 78 MPa.

The experimental data for oil-saturated sandstone are given by Winkler (1985, Figs 3 and 4, and Tables 4 and 7). It is important to understand how the data were

Table 1. Material properties of dry Berea sandstone.

Grain	$\rho_s = 2650\,\mathrm{kg/m^3}$
	$K_s = 37\,\mathrm{GPa}$
Matrix	$K_m = 15.45\,\mathrm{GPa}$
	$\mu_m = 13.48\,\mathrm{GPa}$
	$\phi = 0.203$
	$\mathscr{T} = 2$
	$\kappa = 10^{-12}\,\mathrm{m^2}$
	$\alpha_p = 2\times 10^{-4}{}^\circ\mathrm{C}^{-1}$

1 cP = 0.001 Pa s.

measured. After a suitable pore vacuum was achieved, the confining pressure was increased to 40 MPa. Dry-rock wave velocities were then obtained at successive pressures as the confining pressure decreased to 10 MPa. While still in the pressure vessel, the sample was saturated with oil to a pore pressure of 5 MPa. The differential pressure p_d was then increased to 10, 20 and 40 MPa, corresponding to the values $(p_c, p) = (20, 10)$, (40,20) and (60,20) (in MPa). Note that Winkler (1985) refers to the differential pressure as the effective stress. The experiments on dry samples correspond to zero pore pressure. Best-fit plots of the dry-rock compressibility and shear modulus versus confining pressure are

$$K_m^{-1}[\mathrm{GPa}^{-1}] = 0.064 + 0.122\exp(-p_c[\mathrm{MPa}]/6.48), \tag{45}$$

$$\mu_m[\mathrm{GPa}] = 13.7 - 8.5\exp(-p_c[\mathrm{MPa}]/9.14), \tag{46}$$

and c_p in GPa^{-1} is given by (14), with $c_p^\infty = 0.155$, $\beta = 0.6$, $p^\star = 6.48$. The pore compressibility c_p has been obtained from (27) by assuming that the porosity is that at hydrostatic pore pressure (this approximation is supported by experimental data obtained by Domenico (1977) and Han, Nur and Morgan (1986). The best-fit plots for c_p and K_m^{-1} are illustrated in Fig. 1. The error bars are obtained from (27) and (28) by simple error analysis, assuming that P-wave and S-wave velocities are accurate to within 1% and 2%, respectively (Winkler 1985).

In order to obtain the moduli for different combinations of the confining and pore pressures we should make the substitution $p_c \rightarrow p_e = p_c - n(p_H + \Delta p)$, where we

Table 2. Properties of pore fluids.

Fluid	Bulk modulus (GPa)	Density ($\mathrm{kg/m^3}$)	Viscosity (cP)	Thermal expansion ($^\circ\mathrm{C}^{-1}$)
Light oil	0.57	700	10	5×10^{-4}
Winkler's oil	2.16	890	240	5×10^{-4}
Heavy oil	2.2	970	850	7.7×10^{-4}
Water	2.25	1040	1.8	5×10^{-4}

1 cP = 0.001 Pa s.

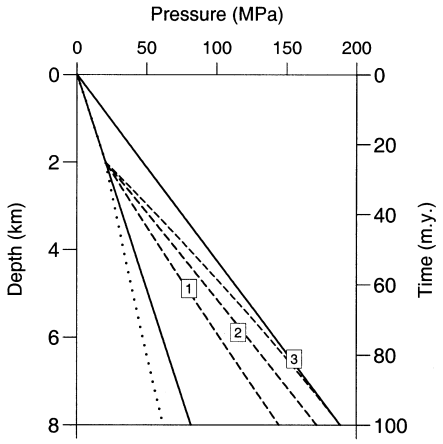

Figure 2. Pore-pressure build-up with depth for different pore fluids, where the continuous lines represent the hydrostatic and lithostatic pressures. The dotted line corresponds to full light-oil saturation, and the broken lines to full Winkler's (1985) oil saturation (label 1), partial saturation ($S_{wi} = 0.5$ and heavy oil) (label 2), and full heavy-oil saturation (label 3).

assume, following Gangi and Carlson (1996), that n depends on differential pressure as

$$n = n_0 - n_1 p_d, \qquad n_0 = 1, \qquad n_1 = 0.014\,\mathrm{MPa}^{-1}.$$

This dependence of n versus differential pressure is in good agreement with the experimental values corresponding to the compressional-wave velocity obtained by Christensen and Wang (1985) and Prasad and Manghnani (1997).

Table 1 indicates the properties of dry Berea sandstone, where the values correspond to those at the initial (hydrostatic) pore pressure. The pore-fluid properties are given in Table 2. The pore-pressure build-up with depth for different pore fluids is shown in Fig. 2, where the continuous lines represent the hydrostatic and lithostatic pressures. The dotted line corresponds to full light-oil saturation, and the broken lines to full Winkler's (1985) oil saturation (label 1), partial saturation ($S_{wi} = 0.5$ and heavy oil) (label 2), and full heavy-oil saturation (label 3). As can be appreciated, the rock is underpressured for full light-oil saturation and increasing pore-fluid bulk modulus gives overpressure. For low compressibilities and high thermal expansion coefficients of the pore fluid, the pore pressure may exceed the lithostatic pressure. In the case of heavy oil, the cause is the high thermal expansion coefficient.

Figure 3 shows (a) the low-frequency (25 Hz) and (b) the ultrasonic (1 MHz) compressional- and shear-wave velocities versus differential pressure p_d for heavy oil (continuous line) and Winkler's (1985) oil (broken and dashed lines). The dotted line corresponds to the range 0 to 2 km, where the rock is normally pressured (see Fig. 2); the black squares and empty circles are the experimental compressional- and

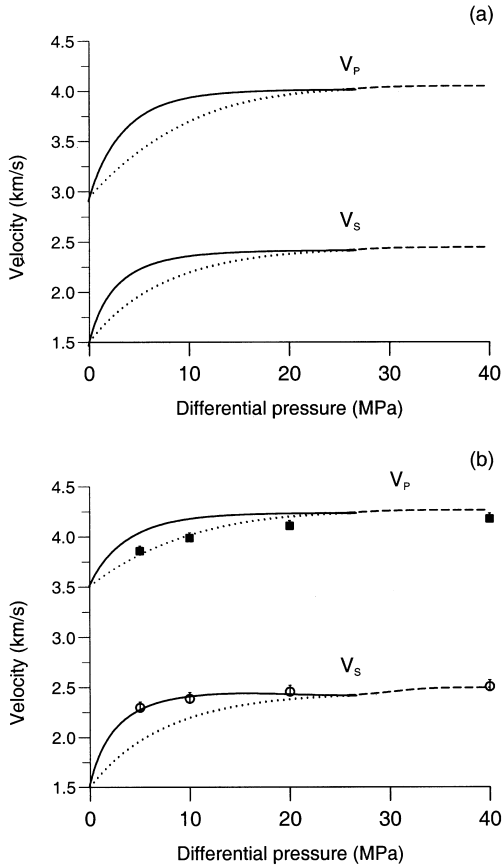

Figure 3. Low-frequency (25 Hz) (a) and ultrasonic (1 MHz) (b) compressional- and shear-wave velocities versus differential pressure p_d for heavy oil (continuous line) and Winkler's (1985) oil (broken and dashed lines). The dotted line corresponds to the range 0 to 2 km, where the rock is normally pressured (see Fig. 2). The black squares and empty circles are the experimental compressional- and shear-wave velocities obtained by Winkler (1985) for oil-saturated Berea sandstone. P-wave and S-wave velocities are accurate to within 1% and 2%, respectively.

shear-wave velocities obtained by Winkler (1985) for oil-saturated Berea sandstone. We use a continuous spectrum of dissipation mechanisms for M_c, from 1 Hz to 1 MHz and $\bar{Q} = 14.55$, regardless of the saturations. The pore fluid affects mainly the compressional-wave velocity, with unrelaxed velocities (1 MHz) higher than relaxed velocities (25 Hz), as expected. The decrease in wave velocity at low differential pressures is due to the unconsolidation effect, implicitly contained in (45) and (46). From 2 to 8 km (continuous lines) the cause is overpressuring, and from 0 to 2 km (dotted lines) the cause is the pore pressure approaching the confining pressure at very shallow depths, since in this case the rock is normally pressured. At deep depths,

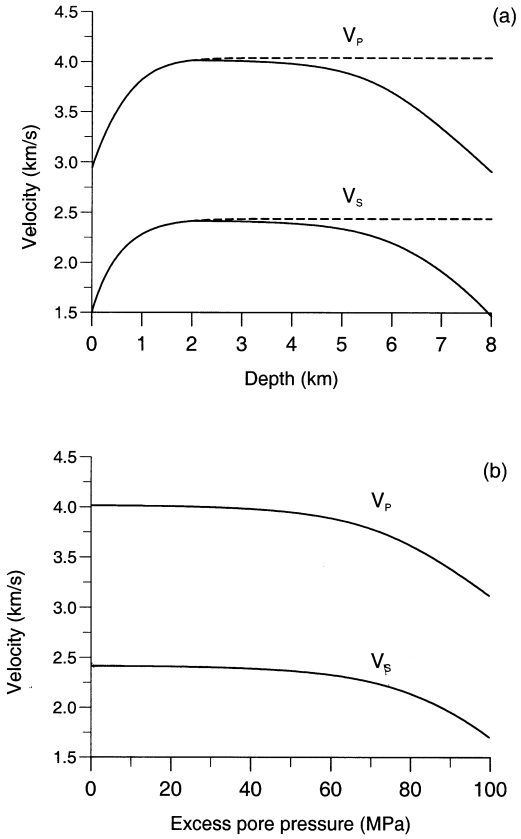

Figure 4. Seismic (25 Hz) compressional- and shear-wave velocities of Berea sandstone saturated with heavy oil versus depth (a) and excess pore pressure (b). The broken line represents the wave velocities for the normally pressured rock, i.e. assuming an open 'system'.

the wave velocities decrease substantially when the pore pressure approaches the confining pressure, as is the case for full heavy-oil saturation. This can be appreciated in Fig. 4, where the seismic compressional- and shear-wave velocities of Berea sandstone saturated with heavy oil are represented versus depth (a) and excess pore pressure, $p - p_H$, (b). The rock has been compacted by the overburden at 2 km depth. The unconsolidation due to disequilibrium compaction then starts, until the pore fluid reaches the confining pressure at approximately 8 km. Note the differences from the velocities obtained for a normally pressured rock (broken lines).

The seismic (a) and ultrasonic (b) P-wave quality factors versus differential pressure for water-saturated Berea sandstone ($S_{wi} = 1$) are shown in Fig. 5, where the black squares are the experimental values (parallel to the bedding plane) obtained by Prasad and Manghnani (1997). The low-frequency curve is obtained under the assumption of a constant quality factor from the seismic to the ultrasonic band. As

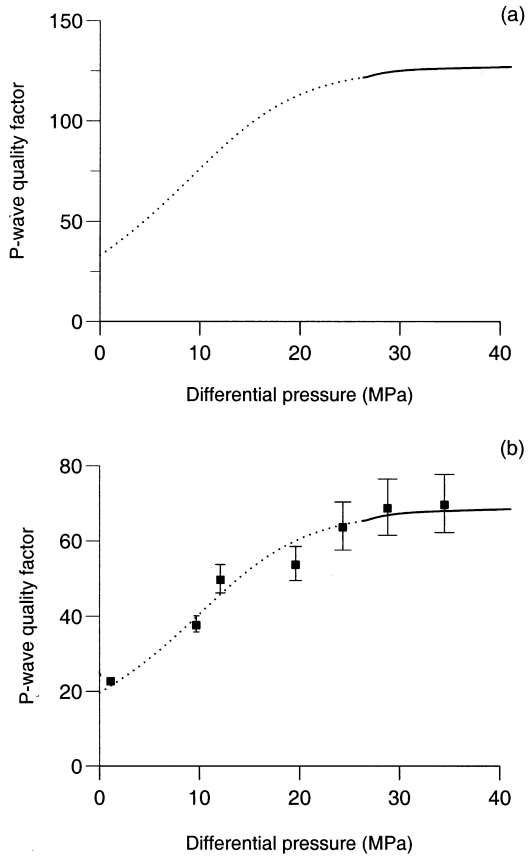

Figure 5. Low-frequency (25 Hz) (a) and ultrasonic (1 MHz) (b) quality factors versus differential pressure for water-saturated Berea sandstone ($S_{wi} = 1$). The dotted line corresponds to the range 0 to 2 km, where the rock is normally pressured, and the continuous lines to the range 2 to 8 km, where the rock is overpressured. The black squares are the experimental bedding-parallel quality factors obtained by Prasad and Manghnani (1997) for Berea sandstone.

before, the dotted line corresponds to the range 0 to 2 km, where the rock is normally pressured, and the continuous lines to the range 2 to 8 km, where the rock is overpressured. Since Prasad and Manghnani (1997) do not provide any information about the error, we consider the error estimated in a similar experiment performed by Peacock *et al.* (1994), where the attenuation coefficient $\bar{\alpha}$ is accurate to 10 dB/m. Since $Q_P \approx 8.6\,\pi f/(c_{P+}\bar{\alpha})$, the corresponding error in Q_P is $\Delta Q_P = Q_P^2 c_{P+}\Delta\bar{\alpha}/(8.6\pi f)$. The value $\bar{Q} = 14.55$ indicated above was chosen to fit the experimental points. As in the case of the wave velocities, the quality factor is not sensitive to overpressure when the pore fluid is water or Winkler's oil.

Figure 6 shows the seismic (a) and ultrasonic (b) P-wave quality factors versus excess pore pressure for Berea sandstone saturated with heavy oil. The quality factor

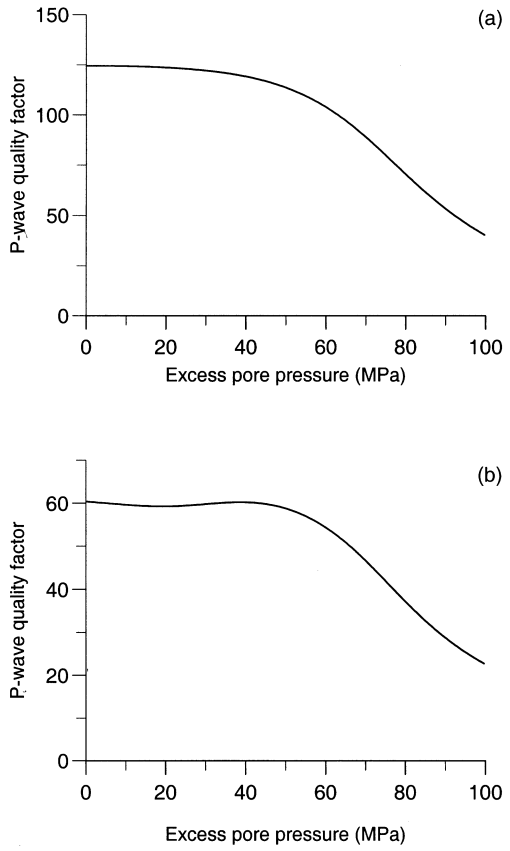

Figure 6. Low-frequency (25 Hz) (a) and ultrasonic (1 MHz) (b) quality factors versus excess pore pressure for Berea sandstone saturated with heavy oil.

is assumed to be constant, with $\bar{Q}$ the same as in the previous example. Overpressure implies low quality factors and therefore high wave dissipation. The quality factor can be a good indicator of excess pressure provided that reliable estimates can be obtained at seismic frequencies.

Conclusions

Non-equilibrium compaction generates abnormal fluid pressures that, under certain conditions, can be detected with seismic methods. This is very important in drilling applications. The results for a model in which a reservoir volume is buried at a constant sedimentation rate for a geothermal gradient, which is constant in both time and depth, show that wave velocities and quality factors decrease with decreasing differential pressure (or effective pressure). The large change is due mainly to the fact that the dry-rock moduli are functions of the effective pressure, with the largest changes

occurring at low differential pressures. For a given pore-space compressibility, the fluid mixture filling the pore space has a major influence on P-wave velocity and may cause underpressure or overpressure depending on its compressibility and thermal expansion coefficient. Rocks saturated with fluids of high compressibility and low thermal expansion coefficient are generally underpressured, and rocks saturated with fluids of low compressibility and high thermal expansion coefficient are generally overpressured, and can be seismically 'visible'. At high differential pressures the velocities are almost constant. Perceptible changes in the velocities occur when the differential pressure decreases to 20 MPa and they become significant when the differential pressure decreases to about 15 MPa. The quality factor curve for full water saturation calculated with the present model is in good agreement with experimental values obtained at the ultrasonic frequency band. The model is able to predict pore pressure from seismic properties if reliable estimates of wave velocities and quality factor can be obtained.

Acknowledgements

This work was supported by Norsk Hydro a.s. (Bergen) with funds from the Source Rock project, and by the European Union under the project 'Detection of overpressure zones with seismic and well data'. We thank Hans Helle for important technical comments.

References

Batzle M. and Wang Z. 1992. Seismic properties of pore fluids. *Geophysics* **57**, 1396–1408.

Berryman J.G., Thigpen L. and Chin R.C.Y. 1988. Bulk elastic wave propagation in partially saturated porous solids. *Journal of the Acoustical Society of America* **84**, 360–373.

Bredehoeft J.D. and Hanshaw B.B. 1968. On the maintenance of anomalous fluid pressures: I. Thick sedimentary sequences. *Geological Society of America Bulletin* **79**, 1097–1106.

Carcione J.M. 1998. Visco-elastic effective rheologies for modelling wave propagation in porous media. *Geophysical Prospecting* **46**, 249–270.

Christensen N.I. and Wang H.F. 1985. The influence of pore pressure and confining pressure on dynamic elastic properties of Berea sandstone. *Geophysics* **50**, 207–213.

Dasios A., Astin T.R. and McCann C. Compressional-wave attenuation from full waveform sonic data. 60th EAGE conference, Leipzig, Germany, Extended Abstracts, 10–44.

Dasios A., Astin T.R. and McCann C. Increasing confidence in seismic Q measurements: a comparison of estimates from sonic and surface seismic data. 68th SEG meeting, New Orleans, USA, Expanded Abstracts, 1080–1083.

Domenico S.N. 1977. Elastic properties of unconsolidated porous sand reservoirs. *Geophysics* **42**, 1339–1368.

Dutta N.C. Shale compaction and abnormal pore pressures: a model of geopressures in the Gulf of Mexico Basin. 53rd SEG meeting, Las Vegas, USA, Expanded Abstracts, S20-2.

Dutta N.C. and Levin F.K. Geopressure. Geophysical Reprint Series No. 7. Society of Exploration Geophysicists.

Gangi A.F. and Carlson R.L. 1996. An asperity-deformation model for effective pressure. *Tectonophysics* **256**, 241–251.

Gist G.A. 1994. Fluid effects on velocity and attenuation in sandstones. *Journal of the Acoustical Society of America* **96**, 1158–1173.

Hague P.S. 1981. Measurements of attenuation from vertical seismic profiles. *Geophysics* **46**, 1548–1558.

Han D., Nur A. and Morgan D. 1986. Effects of porosity and clay content on wave velocities in sandstones. *Geophysics* **51**, 2093–2107.

Helle H.B., Inderhaug O.H., Kovaliev V.P., Madatov A. and Mitrofanov G.M. Complex seismic decomposition – application to pore pressure prediction. 55th EAEG meeting, Stavanger, Norway, Expanded Abstracts, B005.

Mann D.M. and Mackenzie A.S. 1990. Prediction of pore fluid pressures in sedimentary basins. *Marine and Petroleum Geology* **7**, 55–65.

Mavko G. and Mukerji T. 1995. Seismic pore space compressibility and Gassmann's relation. *Geophysics* **60**, 1743–1749.

Peacock S., McCann C., Sothcott J. and Astin T.R. 1994. Experimental measurements of seismic attenuation in microfractured sedimentary rock. *Geophysics* **59**, 1342–1351.

Prasad M. and Manghnani M.H. 1997. Effects of pore and differential pressure on compressional wave velocity and quality factor in Berea and Michigan sandstones. *Geophysics* **62**, 1163–1176.

Rubey W.W. and Hubbert M.K. 1959. Role of fluid pressure mechanics of overthrust faulting, II. Overthrust belt in geosynclinal area of Western Wyoming in light of fluid pressure hypothesis. *Bulletin of the Geological Society of America* **70**, 167–205.

Smith J.E. 1971. The dynamics of shale compaction and evolution of pore-fluid pressure. *Mathematical Geology* **3**, 239–263.

Winkler K.W. 1985. Dispersion analysis of velocity and attenuation in Berea sandstone. *Journal of Geophysical Research* **90**, 6793–6800.

Zimmerman R.W., Somerton W.H. and King M.S. 1986. Compressibility of porous rocks. *Journal of Geophysical Research* **91**, 12 765–12 777.